Implications of Styrenic Triblock Copolymer Gel Mechanics on Midblock Bridging Fraction

Kenneth P. Mineart,[1,] Matthew J. Vallely,[1] Lucas A. Rankin,[1] Duncan M. Hill,[1] Byeongdu Lee[2]*

[1]Department of Chemical Engineering, Bucknell University, Lewisburg, PA 17837, USA
[2]X-Ray Science Division, Argonne National Laboratory, Lemont, IL 60439, USA

KEYWORDS

physical gels, block copolymers, bridging fraction

ABSTRACT

Triblock copolymer gels have garnered considerable scientific interest over the past few decades and are used in a variety of applications including consumer cushioning, pressure-sensitive adhesives, and ballistics gels. While many of their applications rely upon understanding mechanical properties, mechanical studies of block copolymer gels are relatively disjointed with each focusing on specific copolymers, which inherently have a fixed molecular weight and composition. The present study examines the quasistatic mechanical response of styrenic triblock copolymer gels composed of seven unique triblock copolymers at various concentrations. Resultant stress-extension data is fitted with the slip-tube network (STN) theory that describes gel mechanics based upon crosslinked network (G_c) and chain entanglement (G_e) modulus contributions. Collectively, modulus contributions imply that midblock bridging is independent of copolymer identity (*i.e.*, molecular weight and block fraction) and dependent on triblock copolymer concentration via $F_b \propto \phi_{ABA}^{0.91\pm0.39}$ over the concentration range examined (ϕ_{ABA} = 0.05-0.39). Gels composed of a complementary diblock-triblock copolymer pair were subsequently analyzed to explore the influence of interlocking loop-loop and loop-bridge pairs within the effective midblock bridging population. These results point to the presence of a physically significant quantity of interlocked loops, but quantitative analysis was inconclusive.

INTRODUCTION

Physically-crosslinked block copolymer gels have been of interest over the past few decades starting not long after styrenic triblock copolymers could be produced on a commercial scale.[1,2] Over this period, the list of block copolymer gel applications has continually grown and now includes consumer cushioning,[3,4] cable filler material,[5] pressure-sensitive adhesives,[6] ballistics gel,[7] biomedical implants,[8,9] and drug delivery media.[10,11] In parallel, studies have focused on the properties of block copolymer gels in order to both inform their use in the aforementioned practices and to establish connections between their molecular-level physics and observable properties. The bulk of these structure-property relationship studies focus on understanding the nanometer-scale periodicity of domains within gels[12–14] and on gels' dynamic rheological response.[15–17] While a few others have considered the quasistatic mechanical behavior of block copolymer gels,[18–20] these instances are often to inform a specific application of focus.[21–24]

Physically-crosslinked block copolymer gels in their most basic form consist of an ABA triblock copolymer and a B-selective solvent. Upon equilibration of the two components, the copolymers' A endblocks microphase segregate into discrete domains whereas the copolymers' B midblocks and B-selective solvent mix to comprise the continuous phase (Figure 1). The copolymer midblocks within this infrastructure can adopt one of two conformations: (*i*) a *loop* wherein both ends of the midblock are confined to the same discrete domain or (*ii*) a *bridge* wherein the midblock ends are confined to two separate discrete domains (Figure 1). Beyond these one-midblock conformations, it has been suggested that two-midblock conformations may be present depending on copolymer concentration. Specifically, interlocked loop-loop and loop-bridge pairs would result in one, or two, looped midblocks serving as *effective bridges* (Figure 1).[25] A gel results in ABA copolymer/B-selective solvent mixtures when enough effective midblock bridges

are present to create a system-spanning network of discrete A domains and the discrete A domains are glassy, or crystalline, at room temperature so that they are mechanically-robust. In this scenario, the discrete domains behave as nanometer-size physical crosslinks.

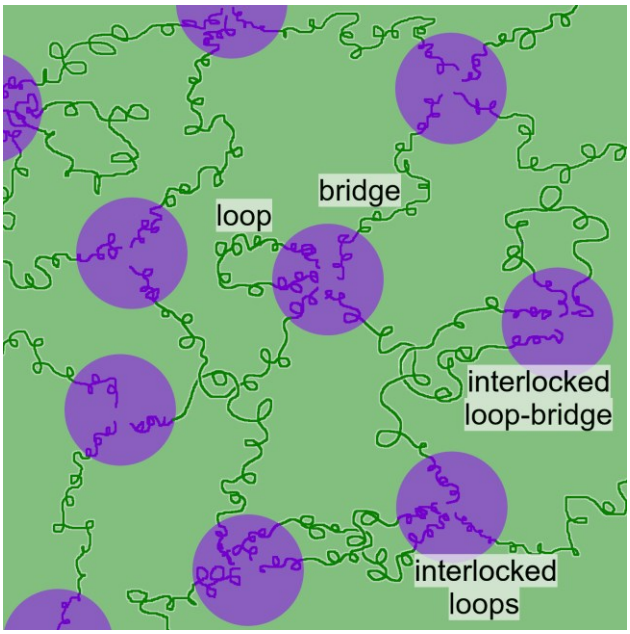

Figure 1. Schematic illustration of ABA triblock copolymer network including various one- and two-midblock conformations: loop, bridge, interlocked loops, and interlocked loop-bridge (each labeled). Solvent molecules, which occupy the continuous phase alongside copolymer midblocks, are not shown for clarity.

Various theories, which were originally developed for pure polymer networks, have been used to describe the mechanics of block copolymer networks and gels.[17,26–28] In particular, the slip-tube network (STN) model[29] is derived based on molecular principles rather than empirical constants and takes the form

$$\sigma_{eng} = \left(G_c + \frac{G_e}{0.74\lambda_{zz}+0.61\lambda_{zz}^{-0.5}-0.35}\right)\left(\lambda_{zz} - \frac{1}{\lambda_{zz}^2}\right) \quad (1)$$

where σ_{eng} is engineering stress, λ_{zz} is extension ratio (*i.e.*, the ratio of sample length at any time to that initially), and G_c and G_e are the crosslinked network and chain entanglement modulus contributions, respectively. The structure of block copolymer gels (as portrayed in Figure 1)

necessitates modification of the STN model since they contain 'hard' discrete domains not included in the original derivation. For example, consideration of spherical discrete domains as nanoparticle fillers leads to an anticipated modulus inflation[30]

$$G_i^{\dagger} = G_i(1 + 2.5\phi + 14.1\phi^2) \tag{2}$$

where $G_i^{\dagger}$ is the effective modulus contribution ($G_c^{\dagger}$ or $G_e^{\dagger}$), G_i is the true modulus contribution (G_c or G_e), and ϕ is the volume fraction of filler in the gel, which is equivalent to the A endblock volume fraction, ϕ_A, in the systems under consideration. Combining Equations 1 and 2 yields the overarching expression applicable to block copolymer gels' mechanical behavior:

$$\sigma_{eng} = \left(G_c + \frac{G_e}{0.74\lambda_{zz} + 0.61\lambda_{zz}^{-0.5} - 0.35}\right)\left(\lambda_{zz} - \frac{1}{\lambda_{zz}^2}\right)(1 + 2.5\phi_A + 14.1\phi_A^2) \tag{3}$$

Along with the hard domain 'filler factor' effect described by Equation 2, the molecular principles inherent to the modified STN model are evident from the theoretical definitions of the two modulus contributions.

First, the crosslinked network contribution for a polymer gel, which stems from affine network theory, is defined by

$$G_c = \nu k_B T (d_{AA}/R_{ee})^2 \tag{4}$$

where ν is the number density of elastically effective midblock chains, k_B is Boltzmann's constant, T is absolute temperature, d_{AA} is the distance between crosslink domains, and R_{ee} is the midblock equilibrium end-to-end distance.[27,29] Furthermore, elastically effective midblock chains are those that form bridges between crosslink domains (whether explicitly or through interlocked looping conformations) and their number density can be calculated by

$$\nu = \phi_{ABA} F_b \left(\frac{f_B N \rho_{ABA}}{M_B}\right) \tag{5}$$

where ϕ_{ABA} is the triblock copolymer volume fraction in the gel, F_b is the fraction of midblocks that serve as effective bridges, f_B is the weight fraction of the midblock in the copolymer, N is Avogadro's number, ρ_{ABA} is the triblock copolymer density, and M_B is the copolymer midblock molecular weight. The second modulus contribution, that from midblock entanglements, is defined by

$$G_e = {\phi_{ABA}}^{2.25} F_b \left(\frac{f_B N \rho_{ABA}}{M_{e,B}}\right) k_B T \quad (6)$$

where $M_{e,B}$ is the molecular weight between entanglements of the copolymer midblocks.[27,29] The presence of F_b in Equation 6 is necessary when considering quasistatic experiments since the only entanglements probed are those of the effectively bridged midblocks. Relative to the applied extension rates, non-interlocked loops relax quickly and have a negligible impact whereas bridged chains do not possess the conformational freedom to relax over any time period.[31,32]

It is clear from Equations 3-6 that both copolymer (f_B, M_B, ρ_{ABA}) and formulation (ϕ_{ABA}, ϕ_A) parameters play a pivotal role in theoretically describing gels' quasistatic mechanical behavior. Furthermore, it has been previously noted that changes in ϕ_{ABA} effect the conformational distribution of copolymer midblocks (*i.e.*, F_b).[19,33,34] The objective of the present study is to use quasistatic mechanical data from block copolymer gels' to better understand relationships between copolymer/formulation parameters and midblock bridging fraction.

EXPERIMENTAL SECTION

Materials

Examined gels were formulated with white aliphatic mineral oil (MO) (Hydrobrite 200 PO, Sonneborn) and one of seven styrenic ABA triblock copolymers (two *G* grades from Kraton Polymers and five Septon grades from Kuraray Inc). Select gels also included an AB diblock

copolymer (Septon grade from Kuraray Inc.). Copolymers vary in terms of their molecular weight (M_w), styrenic endblock weight fraction (f_S), and B block chemistry (EB = ethylene-*co*-butylene; EP = ethylene-*co*-propylene; EEP = ethylene/ethylene-*co*-propylene) (Table 1). They are labeled to capture the majority of this information. For example, $S_{22}EB_{114}S_{22}$ refers to a triblock copolymer with ≈22 kg/mol styrenic endblocks and a ≈114 kg/mol ethylene-*co*-butylene midblock (for a total M_w = 158 kg/mol and f_S = 0.278).

Table 1. Characteristics of block copolymers used in the current study: weight-averaged molecular weight, M_w, molecular mass dispersity, $Đ_M$, polystyrene mass fraction, f_S, and ethylene, propylene, and butylene compositions of each copolymer's midblock.

polymer	***M_w* (kg/mol)***	***f_S* (wt%)†**	**midblock composition (wt%)†,‡**		
			ethylene	***propylene***	***butylene***
$S_{22}EB_{114}S_{22}$	157.5 ± 7.9	27.8	56.8	-	43.2
$S_{36}EB_{162}S_{36}$	234.9 ± 8.1	30.9	59.3	-	40.7
$S_{25}EP_{236}S_{25}$	286.0 ± 12.0	17.5	39.4	60.6	-
$S_{23}EP_{196}S_{23}$	241.1 ± 3.7	18.8	35.1	64.9	-
$S_{37}EP_{174}S_{37}$	247.8 ± 2.9	29.7	38.9	61.1	-
$S_{17}EEP_{95}S_{17}$	129.0 ± 4.6	26.0	61.1	38.9	-
$S_{61}EEP_{298}S_{61}$	421.0 ± 18.0	29.1	56.9	43.1	-
$S_{45}EP_{90}$	135.5 ± 2.8	33.4	35.5	64.5	-

*M_w values were determined via static light scattering measurements
†f_i values were determined via H^1-NMR where f_i is f_S, $f_{ethylene}$, $f_{propylene}$, or $f_{butylene}$
‡midblock composition was determined by $f_j/(f_{ethylene} + f_{propylene} + f_{butylene})$ where f_j is $f_{ethylene}$, $f_{propylene}$, or $f_{butylene}$

Gels were prepared by first dissolving desired amounts of copolymer and oil into toluene (ACS grade, VWR) at a 1:20 mass:volume ratio (*e.g.*, 0.2 g $S_{22}EB_{114}S_{22}$ and 0.8 g MO dissolved in 20 mL toluene). Upon full dissolution, toluene was removed via rotary evaporation and the remaining gel product was annealed in a vacuum oven (120-140 °C, 0.05 atm, 18-24 hours). Finally, gels were formed into strips for mechanical measurements using a melt press operated at 100-160 °C

(depending on copolymer concentration and molecular weight) and minimal applied pressure. The resultant strips measured *ca.* 40 mm (length) x 7.6 mm (width) x 1.6 mm (thickness).

Small Angle X-ray Scattering

Small angle x-ray scattering (SAXS) measurements were conducted on beam line 12-ID-B at the Advanced Photon Source (APS) within Argonne National Laboratory. Experiments used 13.3 keV x-ray radiation ($\lambda = 0.93$ Å), a sample-to-detector distance of 2.01 m, and an exposure time of one second. Scattered x-rays were collected using a Pilatus 2M detector, and all measurements were performed at ambient temperature and pressure. Upon confirming isotropic scattering based upon the 2D intensity maps, raw 2D data were converted into 1D profiles via azimuthal integration where the scattering vector magnitude, q, is related to the scattering half-angle, θ, by $q = 4\pi\sin(\theta)/\lambda$. One-dimensional scattering profiles were fit using *SasView*.[35]

Uniaxial Tensile Testing

Uniaxial tensile testing was performed on an ADMET eXpert 8000 planar biaxial tester operated in single-axis mode. A gauge length of 20 mm was used for all experiments and slack created during loading gel samples into the test grips was eliminated prior to the start of tests using a 1-2 kPa preload. The initial length used to determine extension ratio was that following preloading (23-25 mm). Tests of varying extension rate were conducted on select gel formulations to ensure that all of the analyzed experiments were administered quasistatically. The extension rate used in actual quasistatic tests was found to depend primarily on copolymer concentration and varied from 0.01 mm/s ($\approx 5\text{x}10^{-4}$ s^{-1}) to 0.2 mm/s (≈ 0.01 s^{-1}). A minimum of three replicates were tested for each formulation and all experiments were conducted on fresh gel strips. Tensile data was fit with the STN model (Equation 3) using MATLAB.

RESULTS AND DISCUSSION

Structure of Formulated Gels

Block copolymer gels' discrete domains must exhibit a spherical morphology in order for Equations 2 and 3 to be valid. To address this, we consider 1D SAXS profiles for gels composed of each of the triblock copolymers presented in Table 1 at w_{ABA} = 0.05, 0.10, 0.20, 0.30, and 0.40 where w_{ABA} is the weight fraction of copolymer in the gel (and is converted to ϕ_{ABA} via $\phi_{ABA} = w_{ABA}\rho_{gel}/\rho_{ABA}$ where ρ_{gel} is gel density). The majority of the 1D SAXS profiles collected have a similar qualitative shape consisting of two sharper peaks at lower q and several diffuse peaks at intermediate q (Figures 2a and S1). Select gels, particularly those containing higher concentrations of copolymers with higher molecular weights ($S_{61}EEP_{298}S_{61}$ at ϕ_{ABA} = 0.29 and $S_{36}EB_{162}S_{36}$ and $S_{37}EP_{174}S_{37}$ at ϕ_{ABA} = 0.39), deviate from this behavior. We believe this is due to ineffective annealing of these gels based upon the broadening of the profiles' features, but exclude them from further analysis to ensure full validity of Equation 3. Those profiles that exhibit qualitatively anticipated features were fit using the modified hard sphere model, which describes the nanoscale structure of gels as spherical domains with an average radius, r_A (Figure S2a), a hard sphere radius, r_{hs}, and a hard sphere volume fraction, ϕ_{hs}.[36] The two radii can be further converted to the distance between crosslinks, d_{AA}, via $2r_{hs} - 2r_A$ (Figure S2b).

Beyond the qualitative structural confirmation offered by good SAXS fits with the modified hard sphere model, copolymer gels' nanostructure can be quantitatively confirmed by comparing geometric fit parameters to anticipated values based upon molecular and formulation quantities. Specifically, the A-rich domain volume fraction is calculated from SAXS fit parameters as $\phi_{A,SAXS} = \phi_{hs}(4\pi r_A^3/3)/(4\pi r_{hs}^3/3)$ whereas the anticipated A-rich domain volume fraction is determined by $\phi_{A,form} = w_{ABA}f_A(\rho_{gel}/\rho_A)$. Results of these calculations are in outstanding agreement for all gel

formulations fitted with the modified hard sphere model (Figure 2b) further validating the nanostructure determined via SAXS experiments and model fits.

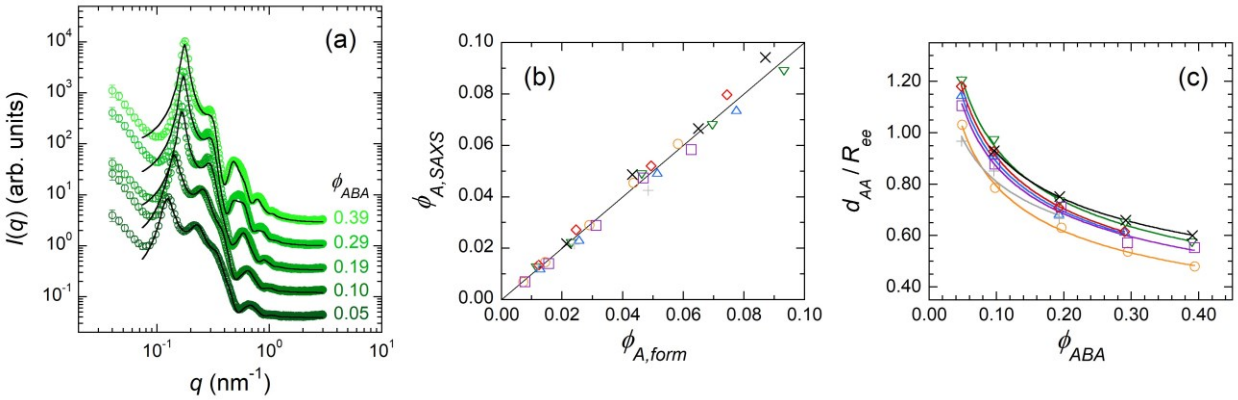

Figure 2. Representative 1D SAXS data for gels containing $S_{22}EB_{114}S_{22}$ at various concentrations (vertically shifted by 3^n for clarity) (a), a comparison between the *A*-rich domain volume fraction computed from SAXS fit parameters, $\phi_{A,SAXS}$, and based on formulated quantities, $\phi_{A,form}$, for examined gels (b), and the midblock stretch ratio, d_{AA}/R_{ee}, for examined gels (c). Symbols in (b) and (c) correspond to $S_{22}EB_{114}S_{22}$, green ▽; $S_{36}EB_{162}S_{36}$, blue △; $S_{25}EP_{236}S_{25}$, orange ○; $S_{23}EP_{196}S_{23}$, purple □; $S_{37}EP_{174}S_{37}$, red ◇; $S_{17}EEP_{95}S_{17}$, black ×; $S_{61}EEP_{298}S_{61}$, gray +. Lines in (a) are modified hard sphere model fits to the data, the line in (b) reflects quantitative agreement between $\phi_{A,SAXS}$ and $\phi_{A,form}$, and lines in (c) are guides to the eye.

One additional piece of structural data necessary for interpreting mechanical behavior is the equilibrium midblock end-to-end distance, R_{ee}, which was calculated for each copolymer via

$$R_{ee} = \sqrt{C_\infty N_{CC} l_{CC}^2}$$

where C_∞ is the Flory characteristic ratio, N_{CC} is the number of C-C bonds along the midblock backbone, and l_{CC} is the C-C bond length (0.154 nm). Flory characteristic ratios were taken as compositional averages for a given copolymer midblock based upon polymer values for ethylene, propylene, and butylene of 6.9, 6.0, and 5.8, respectively. Resultant values are listed in Table S1. These values allow the midblock stretching ratio, d_{AA}/R_{ee}, to be determined and translated to the tension/compression (tension: $d_{AA}/R_{ee} > 1$, compression: $d_{AA}/R_{ee} < 1$) imparted on midblock chains due to their confinement within the nanoscale self-assembly prior to the application of stress. Gels at a given ϕ_{ABA} have fairly similar d_{AA}/R_{ee} ratios, and midblock chains are increasingly compressed

with increasing ϕ_{ABA} (Figure 2c). The midblock stretching ratio is also crucial for full interpretation of quasistatic mechanical data (see Equation 4).

Mechanics of Formulated Gels

With a thorough structural understanding of gels now in place, we turn our attention to the mechanical response of triblock copolymer gels. The copolymers used to formulate these gels vary in total molecular weight from 129 kg/mol to 421 kg/mol and in polystyrene endblock fraction from 0.175 g PS/g to 0.297 g PS/g. Additional copolymers were initially considered to further expand the range of each parameter, but it was observed that gels containing $S_{10}EB_{55}S_{10}$ or $S_{25}EP_{26}S_{25}$ at various concentrations either failed at small extension values (*i.e.*, $\lambda_{zz} \approx 1.2\text{-}1.5$) or formed two macroscopic phases. We hypothesize that these systems do not meet two criteria necessary for homogenous, highly-elastic gel formation. First, $S_{10}EB_{55}S_{10}$ does not have large enough polystyrene endblocks to form mechanically-robust physical crosslinks as indicated by their molecular weight compared with the entanglement molecular weight of polystyrene (16.5 kg/mol).[37] Second, the high endblock fraction and relatively short midblock of $S_{25}EP_{26}S_{25}$ prevent full solubility in aliphatic mineral oil and inhibits formation of an adequate system-spanning network, respectively.

Mechanical test results of validated gel formulations exhibit similar qualitative shape in their stress-extension profiles: a monotonic increase with an initial concave down region that transitions to approximately linear (Figures 3 and S3). Some gels, particularly those with higher concentrations of triblock copolymer, also exhibit an inflection to convex up behavior at higher extension values (Figure 3a). This mechanical response is generally aligned with the STN model. The initial, nonlinear region is explained by the combined effects of the crosslinked network and midblock entanglements. Upon reaching $\lambda_{zz} \approx 2.0$, the contribution from midblock entanglements

becomes roughly constant and the crosslinked network contribution approaches linear (Figure S4). Under high-concentration, high-λ_{zz} conditions wherein the convex-up inflection occurs, we hypothesize that non-affine network deformation and discrete domain impingement come into play (neither of which is accounted for in the STN model).[38] This latter contribution is mostly negligible and, so, the expression in Equation 3 is used to fit all stress-extension data (Figures 3 and S3) with G_c and G_e serving as fitting parameters.

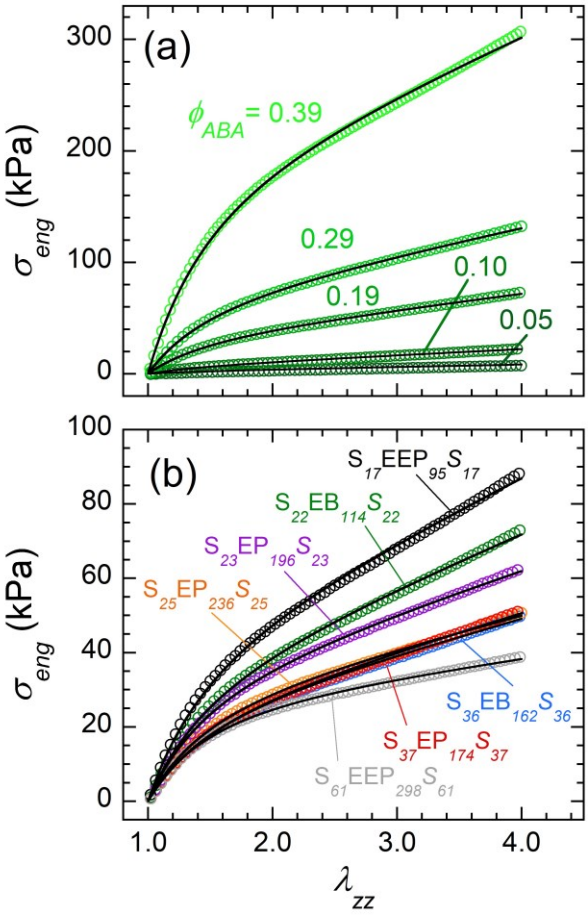

Figure 3. Representative stress-extension data for gels containing a given copolymer, $S_{22}EB_{114}S_{22}$, at various concentrations (labeled, color-coded) (a) or various copolymers (labeled, color-coded) at the same concentration, $\phi_{ABA} \approx 0.19$ (b). Solid lines are STN model fits for each.

Contrasting the stress-extension profiles in more detail, it is clear that increasing copolymer concentration leads to stiffer gels (Figures 3a and S3). Alternatively, an increase in M_w at constant

f_S (compare $S_{22}EB_{114}S_{22}$, $S_{36}EB_{162}S_{36}$, and $S_{61}EEP_{298}S_{61}$ in Figure 3b), or an increase in f_S at constant M_w (compare $S_{23}EP_{196}S_{23}$ and $S_{37}EP_{174}S_{37}$), translates to more compliant (*i.e.*, less stiff) gels. These trends can be better understood by examining the experimentally-fitted modulus contributions in the context of theoretical expectation.

The crosslinked network contribution follows similar trends as those seen in stress-extension profiles: G_c increases with increasing copolymer concentration and decreasing copolymer molecular weight (Figure 4a). However, it can be observed that varying f_S at constant M_w has minimal effect on G_c. These observations align with the theoretical definition (Equations 4 and 5) since increasing ϕ_{ABA} or decreasing M_w (= $M_B/(1\text{-}f_S)$) causes a theoretical increase in G_c whereas f_S appears implicitly in the numerator ($f_B = 1\text{-}f_S$) and denominator ($M_B = (1\text{-}f_S)M_w$) of Equation 5 and therefore is not expected to have a considerable contribution. (Note, ρ_{ABA} is slightly affected by changes in f_S.) To better understand midblock bridging, we normalize the crosslinked network modulus contribution based upon copolymer and nanostructure factors as follows

$$\hat{G}_c = G_c \left[\left(\frac{f_B N \rho_{ABA}}{M_B} \right) k_B T \left(\frac{d_{AA}}{R_{ee}} \right)^2 \right]^{-1} \quad (7)$$

It is anticipated that normalization should isolate the effect of midblock bridging as indicated by combining Equations 4, 5, and 7: $\hat{G}_c = F_b \phi_{ABA}$. It is immediately apparent from experimental data that $\hat{G}_c$ increases superlinearly with ϕ_{ABA} (Figures 4b and S5a), which is explained by dependence of bridging fraction on copolymer concentration.[19,34] We postulate that this relationship can be represented as a power law over the examined concentration range such that $F_b \propto \phi_{ABA}^{\,n}$ and therefore $\hat{G}_c \propto \phi_{ABA}^{\,n+1}$. Fitting data with a power law function then provides the scaling of bridging fraction with copolymer concentration. Fits were initially performed on each individual copolymer series (Figure S5a), and it was found that there is no statistically significant difference between the

power law exponents for these series (ANOVA, $p = 0.102$). This suggests that F_b-ϕ_{ABA} scaling is independent of the copolymer used in gel formulation (*i.e.*, varying f_S and M_w). As a result, all data was globally fit with a power law (Figure 4b) yielding $\hat{G}_c \propto \phi_{ABA}^{2.08\pm0.10}$ (*i.e.*, $F_b \propto \phi_{ABA}^{1.08\pm0.10}$) where the uncertainty reflects a 95% confidence interval.

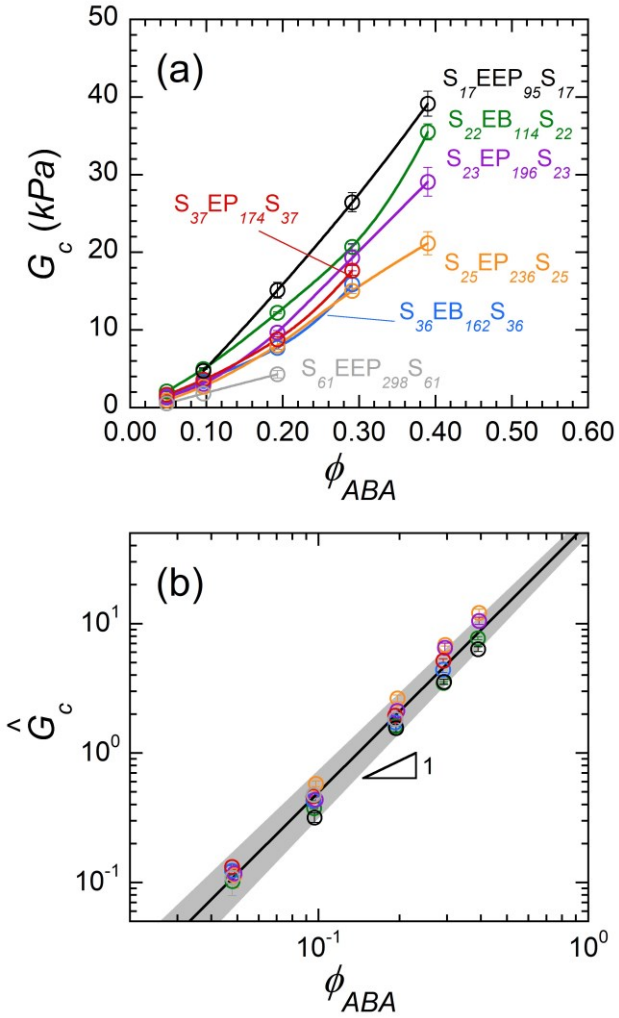

Figure 4. Comparison of crosslinked network modulus contribution, G_c, (a) and normalized G_c, $\hat{G}_c$, (b) for gels composed of various ABA triblock copolymers and copolymer volume fractions. The lines in (a) are guides to the eye for each series whereas that in (b) is a power law fit to all data including the region enclosed by a 95% confidence interval.

The entanglement modulus contribution, G_e, is separately observed to increase with increasing copolymer concentration, or decreasing f_S at fixed midblock composition (compare $S_{25}EP_{236}S_{25}$ and $S_{37}EP_{174}S_{37}$) (Figure 5a). Again, these observations align with theory (see Equation 6) in that

both ϕ_{ABA} and f_S (f_B = 1-f_S) appear as contributing factors. Additional variation in G_e stems from changes in $M_{e,B}$, which is related to midblock composition via[39]

$$\log(M_{e,B}) = f_{et,B}\log(M_{e,et}) + f_{pr,B}\log(M_{e,pr}) + f_{but,B}\log(M_{e,but})$$

where $f_{et,B}$, $f_{pr,B}$, and $f_{but,B}$ are the weight fractions of polyethylene, polypropylene, and polybutylene in the copolymer midblock, respectively, (rightmost columns in Table 1) and $M_{e,et}$, $M_{e,pr}$, and $M_{e,but}$ are the molecular weight between entanglements for polyethylene (1200 g/mol), polypropylene (4600 g/mol), and polybutylene (12300 g/mol), respectively.[40] The role of $M_{e,B}$ can be viewed in experimental data by comparing G_e values for copolymers with similar f_S. For example, $S_{22}EB_{114}S_{22}$ ($M_{e,B}$ = 3281 g/mol) and $S_{36}EB_{162}S_{36}$ ($M_{e,B}$ = 3092 g/mol) have comparable G_e values at a given ϕ_{ABA} whereas $S_{22}EB_{114}S_{22}$ and $S_{17}EEP_{95}S_{17}$ ($M_{e,B}$ = 2024 g/mol) are clearly distinguishable with the latter exhibiting higher values (Figure 5a). Values of $M_{e,B}$ for all copolymers are displayed in Table S2. Like with G_c, the experimentally-fitted G_e values can be normalized to eliminate variation due to copolymer and nanostructure parameters:

$$\hat{G}_e = G_e\left[\left(\frac{f_B N \rho_{ABA}}{M_{e,B}}\right)k_B T\right]^{-1} \quad (8)$$

In this case, it is anticipated that normalization should isolate the effect of midblock bridging in the form of: $\hat{G}_e = F_b\phi_{ABA}^{2.25}$. The experimentally-acquired $\hat{G}_e$ values, again, increase at rate a higher than expected with ϕ_{ABA} (Figure 5b). Using the same postulate as above, power law fitting of data will yield the F_b-ϕ_{ABA} scaling from $\hat{G}_e \propto \phi_{ABA}^{n+2.25}$. Fitting was conducted for each copolymer system individually (Figure S5b) and, like above, no statistically significant difference was noted (ANOVA, p = 0.122). Therefore, fitting was performed globally (Figure 5b) yielding $\hat{G}_e \propto \phi_{ABA}^{2.99\pm0.18}$ (*i.e.*, $F_b \propto \phi_{ABA}^{0.74\pm0.18}$) where the uncertainty reflects a 95% confidence interval.

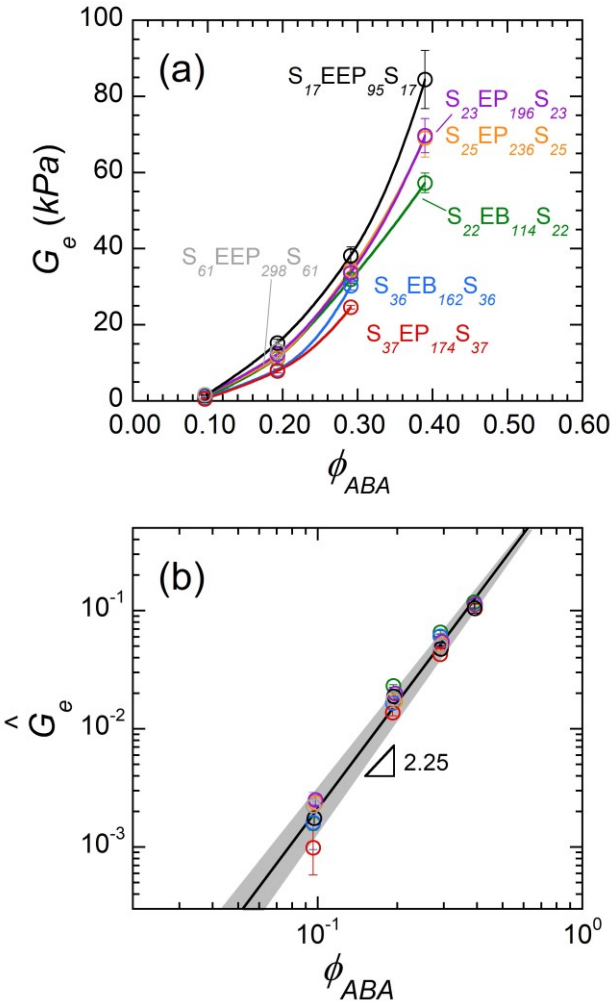

Figure 5. Comparison of chain entanglement modulus contribution, G_e, (a) and normalized G_e, $\hat{G}_e$, (b) for gels composed of various ABA triblock copolymers and copolymer volume fractions. The lines in (a) are guides to the eye for each series whereas that in (b) is a power law fit to all data including the region enclosed by a 95% confidence interval.

Bridging Fraction Discussion

Our data collectively suggests a bridging fraction scaling of $F_b \propto \phi_{ABA}^{0.91\pm0.39}$ for triblock copolymer gels in the concentration range of ϕ_{ABA} = 0.05-0.39 where uncertainty is propagated from those uncertainties determined using G_c and G_e data, as well as, the uncertainty associated with their deviation from one another. For comparison, we fitted others' F_b-ϕ_{ABA} data using power law scaling to extract independent values for the scaling exponent. Watanabe *et al.*[34] probed the looping fractions (and consequently bridging fractions) of midblocks in poly[styrene-*b*-isoprene-

b-styrene] (SIS)/*n*-tetradecane gels over a similar concentration range (*i.e.*, $\phi_{ABA} \approx 0.16\text{-}0.41$) using dielectric relaxation measurements. The SIS copolymer used in their study is fairly small relative to those in the current study (M_n = 50.2 kg/mol), but has a comparable composition (f_S = 28.7 wt%). Sliozberg *et al.*[41] followed up on this work by conducting dissipative particle dynamics (DPD) simulations on comparable gel systems (*i.e.*, coarse-grained $A_1B_6A_1$ copolymer chains in *B*-selective solvent with $\phi_{ABA} \approx 0.16\text{-}0.41$). Finally, Kim and Jo[42] quantified bridging and looping fraction via Monte Carlo simulations on copolymers with an $A_5B_{20}A_5$ architecture in midblock-selective solvent over the concentration range $\phi_{ABA} \approx 0.01\text{-}0.12$. In the latter case, only data from gels with $\phi_{ABA} > 0.05$ were consider for best overlap with the current study. A power law fit represents these others' findings well (Figure S6) and the resultant scaling is in relatively good agreement with that determined here: $F_b \propto \phi_{ABA}^{0.72\pm0.48}$, $F_b \propto \phi_{ABA}^{0.67\pm0.11}$, and $F_b \propto \phi_{ABA}^{0.44\pm0.06}$, respectively, where uncertainties reflect a 95% confidence interval. It is worth noting that the methods used in the referenced studies only count one-midblock bridges in determining F_b whereas the current method also incorporates interlocked loop-loop and loop-bridge pairs. This may provide an explanation for the higher exponent in the present work.

The primary theory used to explain the F_b-ϕ_{ABA} relationship is the translation of increasing copolymer concentration to decreasing crosslink-to-crosslink distance, $d_{A\text{-}A}$.[16,34] Geometric considerations lead specifically to $d_{A\text{-}A} \propto \phi_{ABA}^{-1/3}$, which is evident in our experimental data (Figure S2b). As discussed above, $d_{A\text{-}A}$ defines the end-to-end distance a midblock must adopt in order to bridge two adjacent crosslinks. Bridging midblocks must pay a higher entropic penalty to accommodate a larger $d_{A\text{-}A}$ while those bridging a shorter $d_{A\text{-}A}$ maintain more coiled conformations reducing the entropic penalty. This suggests that higher ϕ_{ABA} leads to lower $d_{A\text{-}A}$ which in turn yields a great number of bridges. One lesser cited explanation for increased effective bridging

fraction is a rise in the interlocked loop midblock population with ϕ_{ABA}. It is anticipated that an increase in the number of midblock chains occupying the continuous phase space would result in more topological entanglements, which is the phenomenon responsible for interlocking loop conformations.

In an attempt to determine whether the latter factor plays a significant role, we formulated several gels with complementary diblock and triblock copolymers (*i.e.*, $S_{37}EP_{174}S_{37}$ and $S_{45}EP_{90}$) at a fixed total copolymer concentration ($\phi_p = \phi_{ABA} + \phi_{AB}$). The intent of this formulation design is to fabricate gels with constant $d_{A\text{-}A}$ but varying ϕ_{ABA}.[15,32] SAXS data were collected for three fixed-ϕ_p series – $\phi_p = 0.10$, $\phi_p = 0.19$, and $\phi_p = 0.29$ – each of which consists of a range of triblock concentration from 50% to 100% of the total (Figures 6a and S7). These data were fitted using the same modified hard sphere model as described above, and the resultant fit parameters (Figure S8a-b) were used for validation by calculating and comparing $\phi_{A,SAXS}$ and $\phi_{A,form}$ (Figure S8c). From these fits, it is observed that values of $d_{A\text{-}A}$, and consequently $d_{A\text{-}A}/R_{ee}$, within each series do not change significantly (Figures 6b and S8d). Any detected changes in bridging fraction would therefore suggest an alternative cause.

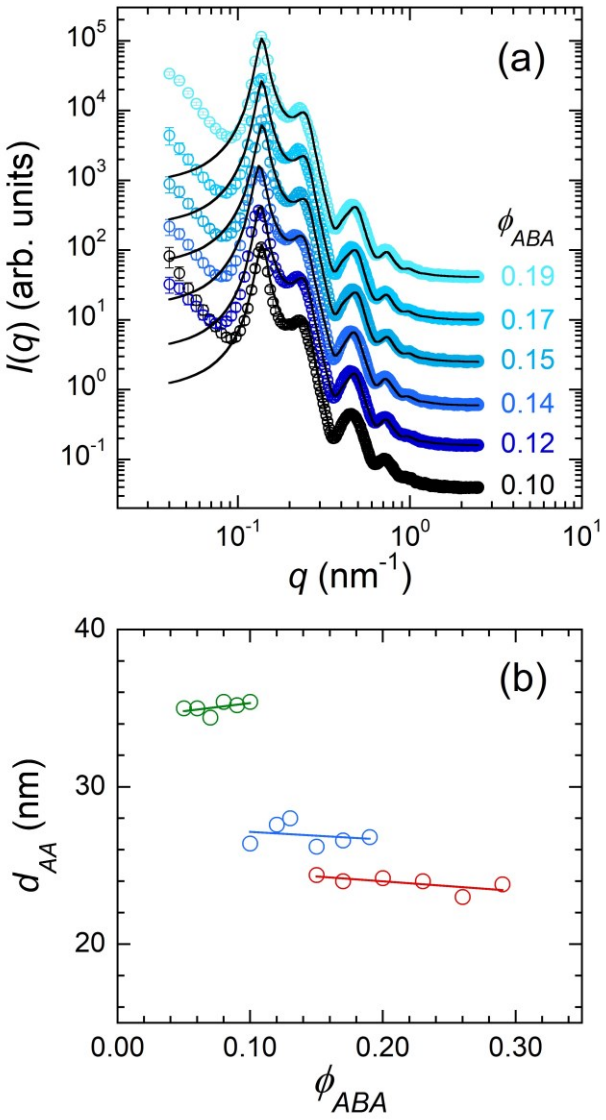

Figure 6. 1D SAXS data from gels composed of $S_{37}EP_{174}S_{37}$ triblock copolymer and $S_{45}EP_{90}$ diblock copolymer at different triblock copolymer concentrations (values indicated on plot) and a fixed total copolymer concentration of $\phi_p = 0.19$ (a), and crosslink-to-crosslink distances for three different fixed-ϕ_p series ($\phi_p = 0.10$ (green), $\phi_p = 0.19$ (blue), and $\phi_p = 0.29$ (red)). Data in (a) are vertically shifted by a factor of 3^n for clarity. Lines in (a) are fits using the modified hard sphere model whereas those in (b) are guides to the eye.

Mechanical tests on diblock-triblock copolymer gels yield stress-extension data for each unique formulation (Figures 7a and S9). Gels within each fixed-ϕ_p series clearly exhibit stiffer mechanical behavior as ϕ_{ABA} is increased. To understand the source of increased stiffness, G_c and G_e were determined for each formulation by fitting data with the STN model (Figures S9 and S10) and

subsequently normalized using Equations 7 and 8, respectively (Figure 7b-c). Note, triblock copolymer parameters (*i.e.*, f_B, ρ_{ABA}, M_B, $M_{e,B}$, R_{ee}) remain the same for all diblock-triblock copolymer gels examined. Additionally, the presence of diblock copolymer chains is not anticipated to have a direct effect on the crosslinked network modulus contribution since the solvent-compatible blocks (*i.e.*, B blocks) are not capable of bridging. Therefore, the trend in $\hat{G}_c$ is still expected to follow the relationship $\hat{G}_c = F_b\phi_{ABA}$. Power law fits to each fixed ϕ_p-series (Figure 7b) are the same within experimental error (ANOVA, $p = 0.665$) and can be represented by $\hat{G}_c \propto \phi_{ABA}^{1.34\pm0.29}$, which translates to $F_b \propto \phi_{ABA}^{0.34\pm0.29}$ based on this expectation.

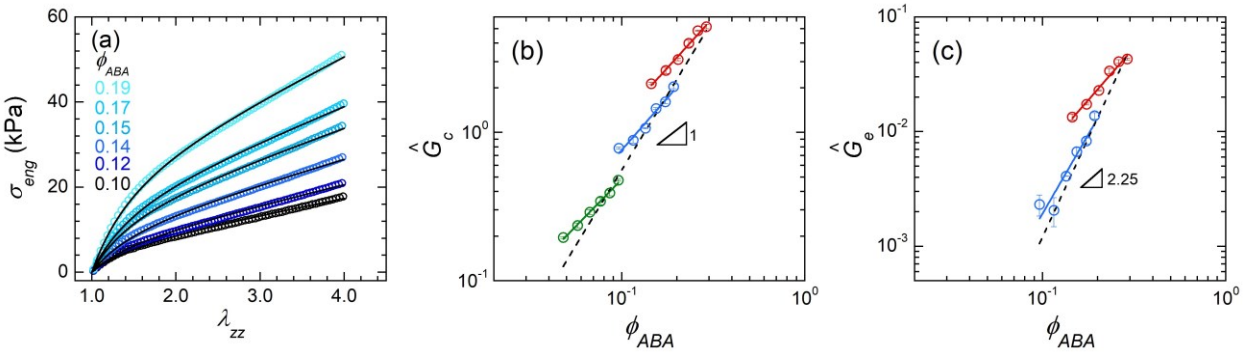

Figure 7. Stress-extension data from gels composed of various $S_{37}EP_{174}S_{37}$ triblock and $S_{45}EP_{90}$ diblock copolymers at different triblock copolymer concentrations (values indicated on plot) and a fixed total copolymer concentration of $\phi_p = 0.19$ (a), as well as, normalized G_c (b) and G_e (c) values from fits ($\phi_p = 0.10$ (green), $\phi_p = 0.19$ (blue), and $\phi_p = 0.29$ (red)). Lines in (a) are fits using the STN model. Solid lines in (b) and (c) indicate power law fits to each fixed-ϕ_p series whereas dashed lines portray fits to pure triblock copolymer gels' data (*i.e.*, $\phi_p = \phi_{ABA}$).

The determined $\hat{G}_e$ values should also remain exclusively dependent on triblock copolymer concentration for the same arguments above yielding $\hat{G}_e = F_b\phi_{ABA}^{2.25}$. However, power law fitting of $\hat{G}_e$ values yields statistically different results (t-test, $p = 0.032$) for the two series analyzed – $\hat{G}_e \propto \phi_{ABA}^{2.49\pm0.92}$ ($\phi_p = 0.19$) and $\hat{G}_e \propto \phi_{ABA}^{1.83\pm0.37}$ ($\phi_p = 0.29$) – and the latter would suggest an inverse relationship between bridging fraction and copolymer concentration: $F_b \propto \phi_{ABA}^{-0.42\pm0.37}$. It is likely that these results are complicated by the B block entanglement effects imparted by the diblock copolymers. While experiments are conducted quasistatically, it is possible that diblock copolymer

midblocks relax very slowly relative to experimental conditions and hence contribute to the extracted $\hat{G}_e$. This notion is supported by the fact that the ϕ_{ABA} dependence is dampened in the higher ϕ_p series (*i.e.*, more diblock copolymers contributing to $\hat{G}_e$) whereas the relationship in the lower ϕ_p series is in closer agreement with $\hat{G}_c$ results (*i.e.*, $F_b \propto \phi_{ABA}^{0.24\pm0.92}$). Dampened scaling of G_e in diblock-triblock systems has similarly been noted by others' from rheological experiments.[15] While $\hat{G}_e$ values are unexpectedly complicated by the presence of diblock copolymers, we believe that $\hat{G}_c$ trends indicate a physically significant rise in the number of interlocked loop-loop and loop-bridge pairs with increasing triblock copolymer concentration. (All uncertainties indicate a 95% confidence interval.)

CONCLUSION

Quasistatic uniaxial tensile experiments shed light on the microscopic structure of block copolymer gels, namely the population of midblock conformations. This is due to the aforementioned experimental techniques' sensitivity to effectively bridged midblock chains. Using tensile data from 30 unique gel formulations, we are able to conclude that the bridging fraction in styrenic triblock copolymer gels scales with copolymer concentration via $F_b \propto \phi_{ABA}^{0.91\pm0.39}$ within the concentration range ϕ_{ABA} = 0.05-0.39. Additionally, this scaling does not vary significantly for copolymers of varying molecular weight or block fractions. The determined scaling exponent is in good agreement with previous studies that directly measure midblock bridging fraction, but is unique in that it includes the contribution from two-midblock bridges – *i.e.*, interlocked loop-loop and loop-bridge pairs. The contribution of interlocked loop-loop and loop-bridge pairs was further explored by testing gels formulated using a complementary diblock and triblock copolymer. These results suggest that interlocked loops account for a physically-significant portion of the midblock population. However, quantitative details could not be confidently extracted due to complexities

arising from the presence of diblock copolymers. Future studies, particularly molecular simulations wherein individual midblock conformations can be calculated/visualized, will be paramount in clarifying the quantity and role of interlocking loop conformations in pure triblock copolymer and diblock-triblock copolymer gels.

ASSOCIATED CONTENT

Supporting Information. The following files are available free of charge. GELMECH_SI.pdf

AUTHOR INFORMATION

Corresponding Author

*Prof. Kenneth P. Mineart, kpm007@bucknell.edu

Author Contributions

The manuscript was written through contributions of all authors. All authors have given approval to the final version of the manuscript.

Funding Sources

NSF Grant Numbers 1904047 and 1828082.

ACKNOWLEDGMENT

This work was supported by the National Science Foundation under Grant No. 1904047 and Grant No. 1828082. We also acknowledge support from the Bucknell University College of Engineering. We would like to thank Kraton Corporation, Kuraray, and Sonneborn for providing the copolymer and aliphatic oil materials used in this study. This research used resources of the Advanced Photon Source, a U.S. Department of Energy (DOE) Office of Science user facility, operated for the DOE

Office of Science by Argonne National Laboratory under Contract No. DE-AC02-06CH11357. Extraordinary facility operations were supported in part by the DOE Office of Science through the National Virtual Biotechnology Laboratory, a consortium of DOE national laboratories focused on the response to COVID-19, with funding provided by the Coronavirus CARES Act.

REFERENCES

(1) Holden, G.; Milkovich, R. Process for the Preparation of Block Copolymers. US3231635A, January 25, 1966.

(2) Condon, N. Block Copolymer Compositions. US3830767A, August 20, 1974.

(3) Delonzor, R. L.; Gentry, J.; Fein, M. E.; Ollerdessen, A. L.; Spero, R. K. Gel Pad Optical Sensor. US5830136 A, November 3, 1998.

(4) Dassler, A. K.; Schwartz, R. M.; Hofeldt, A. J. Cycling Glove Support Area. US8065750 B2, November 29, 2011.

(5) Patel, N. I. Filling Materials for Electrical and Light Waveguide Communications Cables. US4351913 A, September 28, 1982.

(6) Janssen, A.; Endriss, G. Hot Melt Adhesive Compositions for Adherence to Skin and Articles Constructed Therefrom. US6197845B1, March 6, 2001.

(7) Juliano, T. F.; Forster, A. M.; Drzal, P. L.; Weerasooriya, T.; Moy, P.; VanLandingham, M. R. Multiscale Mechanical Characterization of Biomimetic Physically Associating Gels. *J. Mater. Res.* **2006**, *21* (8), 2084–2092. https://doi.org/10.1557/jmr.2006.0254.

(8) Fischenich, K. M.; Lewis, J. T.; Bailey, T. S.; Haut Donahue, T. L. Mechanical Viability of a Thermoplastic Elastomer Hydrogel as a Soft Tissue Replacement Material. *J. Mech. Behav. Biomed. Mater.* **2018**, *79*, 341–347. https://doi.org/10.1016/j.jmbbm.2018.01.010.

(9) Lewis, J. T.; Fischenich, K. M.; Haut Donahue, T. L.; Bailey, T. S. Nanostructure-Driven Replication of Soft Tissue Biomechanics in a Thermoplastic Elastomer Hydrogel. *ACS Biomater. Sci. Eng.* **2018**, *4* (11), 3854–3863. https://doi.org/10.1021/acsbiomaterials.8b00929.

(10) Zhao, Z.; Zhou, Y.; Zhang, C.; Li, Z. Optimization of SIS-Based Hot-Melt Pressure-Sensitive Adhesives for Transdermal Delivery of Hydrophilic Drugs. *Int. J. Adhes. Adhes.* **2016**, *68*, 256–262. https://doi.org/10.1016/j.ijadhadh.2016.04.003.

(11) Gennari, C. G. M.; Quaroni, G. M. G.; Creton, C.; Minghetti, P.; Cilurzo, F. SEBS Block Copolymers as Novel Materials to Design Transdermal Patches. *Int. J. Pharm.* **2020**, *575*, 118975. https://doi.org/10.1016/j.ijpharm.2019.118975.

(12) Mischenko, N.; Reynders, K.; Koch, M. H. J.; Mortensen, K.; Pedersen, J. S.; Fontaine, F.; Graulus, R.; Reynaers, H. Small-Angle X-Ray and Neutron Scattering from Bulk and

Oriented Triblock Copolymer Gels. *Macromolecules* **1995**, *28* (6), 2054–2062. https://doi.org/10.1021/ma00110a045.

(13) Laurer, J. H.; Mulling, J. F.; Khan, S. A.; Spontak, R. J.; Bukovnik, R. Thermoplastic Elastomer Gels. I. Effects of Composition and Processing on Morphology and Gel Behavior. *J. Polym. Sci. Part B Polym. Phys.* **1998**, *36* (13), 2379–2391. https://doi.org/10.1002/(SICI)1099-0488(19980930)36:13<2379::AID-POLB13>3.0.CO;2-0.

(14) Chantawansri, T. L.; Duncan, A. J.; Ilavsky, J.; Stokes, K. K.; Berg, M. C.; Mrozek, R. A.; Lenhart, J. L.; Beyer, F. L.; Andzelm, J. W. Phase Behavior of SEBS Triblock Copolymer Gels. *J. Polym. Sci. Part B Polym. Phys.* **2011**, *49* (20), 1479–1491. https://doi.org/10.1002/polb.22335.

(15) Vega, D. A.; Sebastian, J. M.; Loo, Y.-L.; Register, R. A. Phase Behavior and Viscoelastic Properties of Entangled Block Copolymer Gels. *J. Polym. Sci. Part B Polym. Phys.* **2001**, *39* (18), 2183–2197. https://doi.org/10.1002/polb.1192.

(16) Seitz, M. E.; Burghardt, W. R.; Faber, K. T.; Shull, K. R. Self-Assembly and Stress Relaxation in Acrylic Triblock Copolymer Gels. *Macromolecules* **2007**, *40* (4), 1218–1226. https://doi.org/10.1021/ma061993+.

(17) Mishra, S.; Badani Prado, R. M.; Kundu, S. Concentration-Dependent Mechanical Behavior of Physically Assembled Triblock Copolymer Gels. *ACS Appl. Polym. Mater.* **2020**, *2* (12), 5388–5397. https://doi.org/10.1021/acsapm.0c00583.

(18) Seitz, M. E.; Burghardt, W. R.; Shull, K. R. Micelle Morphology and Mechanical Response of Triblock Gels. *Macromolecules* **2009**, *42* (22), 9133–9140. https://doi.org/10.1021/ma901448x.

(19) Chantawansri, T. L.; Sirk, T. W.; Sliozberg, Y. R. Entangled Triblock Copolymer Gel: Morphological and Mechanical Properties. *J. Chem. Phys.* **2013**, *138* (2), 024908-024908–024910. https://doi.org/doi:10.1063/1.4774373.

(20) Chantawansri, T. L.; Sirk, T. W.; Mrozek, R.; Lenhart, J. L.; Kröger, M.; Sliozberg, Y. R. The Effect of Polymer Chain Length on the Mechanical Properties of Triblock Copolymer Gels. *Chem. Phys. Lett.* **2014**, *612*, 157–161. https://doi.org/10.1016/j.cplett.2014.08.013.

(21) Sudarsan, A. P.; Wang, J.; Ugaz, V. M. Thermoplastic Elastomer Gels: An Advanced Substrate for Microfluidic Chemical Analysis Systems. *Anal. Chem.* **2005**, *77* (16), 5167–5173. https://doi.org/10.1021/ac050448o.

(22) Shankar, R.; Krishnan, A. S.; Ghosh, T. K.; Spontak, R. J. Triblock Copolymer Organogels as High-Performance Dielectric Elastomers. *Macromolecules* **2008**, *41* (16), 6100–6109. https://doi.org/10.1021/ma071903g.

(23) Vargantwar, P. H.; Shankar, R.; Krishnan, A. S.; Ghosh, T. K.; Spontak, R. J. Exceptional Versatility of Solvated Block Copolymer/Ionomer Networks as Electroactive Polymers. *Soft Matter* **2011**, *7* (5), 1651–1655. https://doi.org/10.1039/c0sm01210f.

(24) Mineart, K. P.; Lin, Y.; Desai, S. C.; Krishnan, A. S.; Spontak, R. J.; Dickey, M. D. Ultrastretchable, Cyclable and Recyclable 1- and 2-Dimensional Conductors Based on

Physically Cross-Linked Thermoplastic Elastomer Gels. *Soft Matter* **2013**, *9* (32), 7695–7700. https://doi.org/10.1039/c3sm51136g.

(25) Takano, A.; Kamaya, I.; Takahashi, Y.; Matsushita, Y. Effect of Loop/Bridge Conformation Ratio on Elastic Properties of the Sphere-Forming ABA Triblock Copolymers: Preparation of Samples and Determination of Loop/Bridge Ratio. *Macromolecules* **2005**, *38* (23), 9718–9723. https://doi.org/10.1021/ma050712f.

(26) Seitz, M. E.; Martina, D.; Baumberger, T.; R. Krishnan, V.; Hui, C.-Y.; R. Shull, K. Fracture and Large Strain Behavior of Self-Assembled Triblock Copolymer Gels. *Soft Matter* **2009**, *5* (2), 447–456. https://doi.org/10.1039/B810041A.

(27) Roos, A.; Creton, C. Effect of the Presence of Diblock Copolymer on the Nonlinear Elastic and Viscoelastic Properties of Elastomeric Triblock Copolymers. *Macromolecules* **2005**, *38* (18), 7807–7818. https://doi.org/10.1021/ma050322t.

(28) Yan, J.; Tuhin, M. O.; Sadler, J. D.; Smith, S. D.; Pasquinelli, M. A.; Spontak, R. J. Network Topology and Stability of Homologous Multiblock Copolymer Physical Gels. *J. Chem. Phys.* **2020**, *153* (12), 124904. https://doi.org/10.1063/5.0028136.

(29) Rubinstein, M.; Panyukov, S. Elasticity of Polymer Networks. *Macromolecules* **2002**, *35* (17), 6670–6686. https://doi.org/10.1021/ma0203849.

(30) Guth, E. Theory of Filler Reinforcement. *J. Appl. Phys.* **1945**, *16* (1), 20–25. https://doi.org/10.1063/1.1707495.

(31) de Graaf, A. J.; Boere, K. W. M.; Kemmink, J.; Fokkink, R. G.; van Nostrum, C. F.; Rijkers, D. T. S.; van der Gucht, J.; Wienk, H.; Baldus, M.; Mastrobattista, E.; Vermonden, T.; Hennink, W. E. Looped Structure of Flowerlike Micelles Revealed by 1H NMR Relaxometry and Light Scattering. *Langmuir* **2011**, *27* (16), 9843–9848. https://doi.org/10.1021/la2019605.

(32) Rankin, L. A.; Lee, B.; Mineart, K. P. Effect of Network Connectivity on the Mechanical and Transport Properties of Block Copolymer Gels. *J. Polym. Sci.* **2021**, *59* (1), 34–42. https://doi.org/10.1002/pol.20200695.

(33) Semenov, A. N.; Joanny, J.-F.; Khokhlov, A. R. Associating Polymers: Equilibrium and Linear Viscoelasticity. *Macromolecules* **1995**, *28* (4), 1066–1075. https://doi.org/10.1021/ma00108a038.

(34) Watanabe, H.; Sato, T.; Osaki, K. Concentration Dependence of Loop Fraction in Styrene−Isoprene−Styrene Triblock Copolymer Solutions and Corresponding Changes in Equilibrium Elasticity. *Macromolecules* **2000**, *33* (7), 2545–2550. https://doi.org/10.1021/ma991979f.

(35) Doucet, M.; Cho, J. H.; Alina, G.; Attala, Z.; Bakker, J.; Bouwman, W.; Butler, P.; Campbell, K.; Cooper-Benun, T.; Durniak, C.; Forster, L.; Gonzales, M.; Heenan, R.; Jackson, A.; King, S.; Kienzle, P.; Krzywon, J.; Nielsen, T.; O'Driscoll, L.; Potrzebowski, W.; Prescott, S.; Ferraz Leal, R.; Rozycko, P.; Snow, T.; Washington, A. SasView Version 5.0.3, 2020. https://doi.org/10.5281/zenodo.3930098.

(36) Kinning, D. J.; Thomas, E. L. Hard-Sphere Interactions between Spherical Domains in Diblock Copolymers. *Macromolecules* **1984**, *17* (9), 1712–1718. https://doi.org/10.1021/ma00139a013.

(37) *Polystyrene*. https://polymerdatabase.com/polymers/polystyrene.html.

(38) Matsumiya, Y.; Watanabe, H.; Takano, A.; Takahashi, Y. Uniaxial Extensional Behavior of (SIS)p-Type Multiblock Copolymer Systems: Structural Origin of High Extensibility. *Macromolecules* **2013**, *46* (7), 2681–2695. https://doi.org/10.1021/ma3026404.

(39) Wu, S.; Beckerbauer, R. Chain Entanglement in Homopolymers, Copolymers and Terpolymers of Methyl Methacrylate, Styrene and N-Phenylmaleimide. *Polymer* **1992**, *33* (3), 509–515. https://doi.org/10.1016/0032-3861(92)90727-E.

(40) *Entanglement Spacing*. http://polymerdatabase.com/polymer%20physics/Ne%20Table.html.

(41) Sliozberg, Y. R.; Andzelm, J. W.; Brennan, J. K.; Vanlandingham, M. R.; Pryamitsyn, V.; Ganesan, V. Modeling Viscoelastic Properties of Triblock Copolymers: A DPD Simulation Study. *J. Polym. Sci. Part B Polym. Phys.* **2010**, *48* (1), 15–25. https://doi.org/10.1002/polb.21839.

(42) Kim, S. H.; Jo, W. H. A Monte Carlo Simulation for the Micellization of ABA- and BAB-Type Triblock Copolymers in a Selective Solvent. *Macromolecules* **2001**, *34* (20), 7210–7218. https://doi.org/10.1021/ma0105136.